JOURNAL OF THE KOREAN ASTRONOMICAL SOCIETY
35: 131 ~ 141, 2002

GEMINI NEAR-IR PHOTOMETRY OF THE ARCHES CLUSTER NEAR THE GALACTIC CENTER

YUJIN YANG, HONG SOO PARK, MYUNG GYOON LEE, AND SANG-GAK LEE
Astronomy Program, SEES, Seoul National University, Seoul, 151-742, Korea
E-mail: yjyang@astro.snu.ac.kr, hspark@astro.snu.ac.kr, mglee@astrog.snu.ac.kr and sanggak@astrosp.snu.ac.kr
(Received Aug. 29, 2002; Accepted Sept. 6, 2002)

ABSTRACT

We present Near-IR photometry of the Arches cluster, a young and massive stellar cluster near the Galactic center. We have analyzed the high resolution (FWHM $\sim 0.2''$) H and K' band images in the *Galactic Center Demonstration Science Data Set*, which were obtained with the Gemini/Hokupa's adaptive optics (AO) system. We present the color-magnitude diagram, the luminosity function and the initial mass function (IMF) of the stars in the Arches cluster in comparison with the *HST/NICMOS* data. The IMF slope for the range of $1.0 < \log\ (M/M_{\odot}) < 2.1$ is estimated to be $\Gamma = -0.79 \pm 0.16$, in good agreements with the earlier result based on the *HST/NICMOS* data [Figer et al. 1999, ApJ, 525, 750]. These results strengthen the evidence that the IMF of the bright stars close to the Galactic center is much flatter than that for the solar neighborhood. This is also consistent with a recent finding that the IMFs of the bright stars in young clusters in M33 get flatter as the galactocentric distance decreases [Lee et al. 2001, astro-ph 0109258]. It is found that the power of the Gemini/AO system is comparable, with some limits, to that of the *HST/NICMOS*.

Key words : open clusters and associations: individual (Arches cluster) — stars: luminosity function, mass function

I. INTRODUCTION

The Arches cluster is a very unique cluster in the Milk Way, because it is a very massive and compact young cluster close to the Galactic center. It was confirmed as a star cluster including emission-line stars by Nagata et al (1995). To date only three clusters are known to be very close to the Galactic center. The other two clusters are the Quintuplet cluster and the IRS 16 cluster at the Galactic center. The size of the Arches cluster is about $15''$ (= 0.58 pc at the distance of 8 kpc), and the total mass is estimated to be about $10^4 M_{\odot}$ (Figer et al. 1999). The Arches cluster has a very high peak density $3 \times 10^5\ M_{\odot}\ \mathrm{pc}^{-3}$ in the inner $9''$ (0.35 pc), showing that it is one of the densest known young clusters in the Local Group galaxies. Similar examples are R 136, the central cluster of 30 Dor in the Large Magellanic Cloud and NGC 3603 in our Galaxy. The age of the cluster is estimated to be about 2–5 Myrs (Figer et al. 1999, Blum et al. 2001). Very recently Yusef-Zadeh et al. (2002) detected, using the Advanced CCD Imaging Spectrometer on board Chandra X-Ray Observatory, two X-ray sources in this cluster, and suggested that the X-ray emission from the sources arises from stellar wind sources in the cluster.

The presence of compact young clusters like the Arches cluster and the other two clusters near the Galactic center indicates that stars are forming even in such a dense environment. Therefore a study of these clusters will provide important hints for understanding the star formation process under extreme environments.

Stars in the Arches cluster were studied in detail for the first time by Figer et al. (1999) and Kim et al. (2000) who used the Hubble Space Telescope (*HST*) Near-Infrared Camera and Multiobject Spectrometer (*NICMOS*) observations. Figer et al. (1999) found several interesting results on this cluster: (1) the Arches cluster is very young, with an age of only about 2 Myrs, showing that stars are forming very recently in the region close to the Galactic center; and (2) the initial mass function (IMF) of the massive stars in this cluster is derived to be significantly flat, having a slope of $\Gamma = \log N / \log M = -0.7 \pm 0.1$ for the mass range of $0.8 < \log\ (M/M_{\odot}) < 2.1$. Surprisingly this IMF slope is much flatter than the average for other clusters in the solar neighborhood which is close to the Salpeter value, $\Gamma = -1.35$ (see Scalo 1998). This result shows, if confirmed, that stars with flatter IMFs are formed in the dense region like the Galactic center, while stars with steeper IMFs are formed in the low-density region like the solar neighborhood.

In spite of the importance of the study of these clusters, there are only a few studies of these clusters to date. It has been a demanding job to investigate the IMF for the clusters like the Arches from the ground-based observation, because the cluster fields are very crowded and the interstellar extinction toward the clus-

Corresponding Author: M. G. Lee

ters is severe. Therefore the *HST* remains to be almost the only instrument useful for these studies until recently. However, with the advent of Adaptive Optics (AO) system at the Gemini Telescope, it became possible to study the stars in the clusters like the Arches in detail with ground-based observations.

Table 1. Observation log

ID	Date (2000)	Filter	Total exp. time(sec)	FWHM (″)
1	07-05	H	3	0.140-0.165
2	07-05	H	720	0.180-0.230
3	07-09	K'	2	0.120-0.140
4	07-30	K'	16	0.105-0.135
5	07-04	K'	180	0.185-0.250
6	07-03	K'	240	0.145-0.180
7	07-30	K'	480	0.125-0.145
8	07-09	K'	1020	0.125-0.135

In this paper we present Near-IR photometry of the Arches cluster obtained for science demonstration using the Gemini/AO system in comparison with the *HST/NICMOS* results. Preliminary results of this study were presented by Yang et al. (2002). During the preparation of this paper, Stolte et al. (2002) also presented at a conference a similar study to ours using the same data set.

II. DATA SET AND DATA REDUCTION

(a) Data Set

We have used the data set prepared as part of the *Galactic center demonstration science* which was obtained using Hokupa's Adaptive Optics system at the Gemini/ North telescope in July, 2000. We have analyzed the preprocessed data released to the public. This data set contains deep, high resolution H and K' band (1.65, 2.12 μm) images of the central regions of the Arches cluster. The pixel scale is 0″.02/pixel, giving a total field of view 20″.5 × 20″.5.

Table 1 lists the observation log. The FWHMs of the point sources are measured to be $\sim$ 0.2″ in the H band images, and $\sim$ 0.1″ in the K' band images. Fig. 1. displays gray scale maps of the Gemini images of the Arches clusters in comparison with the *HST/NICMOS* images. The field of view of the Gemini images is smaller than that of the *NICMOS* images, as shown in Fig. 1, but covering the most central region of the cluster. Fig.1 shows that stars in the cluster are very well resolved in the Gemini images.

(b) Data Reduction

We have derived the instrumental magnitudes of the stars in the images using the point spread function fitting package of IRAF /DAOPHOT (Stetson 1987). Because the median sky level was subtracted from the image in the released data set, we added this value to the raw image to derive photometric errors.

Because this data in the Gemini demonstration program was obtained primarily to check the performance of the telescope and instruments and to test the data reduction scheme, this data set has some limitations for detailed study of the Arches cluster. First, the exposure time of the H images is not as deep as K' images. Therefore fewer faint stars are detected in the H images than in the K' images. Second, the field coverage of each exposure is somewhat different, reducing the areas common among the images. Third, the observation for standard stars is not available. However, these images are still the sharpest and deepest images ever taken of this cluster at the ground-based telescope.

Because the observation for standardization was not available for this data set, we have calibrated our photometry using the *HST/NICMOS* data given by Figer et al. (1999). We have transformed the instrumental H and K' magnitudes into the *HST/NICMOS* system using the photometry given by Figer et al. (1999). The effective wavelengths of the *NICMOS* filters F160W and F205W are, respectively, 1.60 and 2.05 μm, which are slightly different from the Gemini filters.

The coordinate transformation equations between the Gemini photometry and the *NICMOS* photometry are derived as follows:

$$X(NIC) = 0.187X(Gem) - 0.187Y(Gem) + 225.421,$$

$$Y(NIC) = -0.189X(Gem) - 0.187Y(Gem) + 490.104$$

where the coordinates are given in units of pixel of the *NICMOS* and the Gemini images, respectively.

Using the bright stars common between the Gemini and *NICMOS* images we have derived the transformation equations as follows:

$$m_{\rm F205W} = k + 0.103\ (h - k) - 0.587,\quad \sigma = 0.058,$$

$$m_{\rm F160W} - m_{\rm F205W} = 0.924\ (h - k) + 1.361,\quad \sigma = 0.062$$

where h and k represent the instrumental magnitudes of Gemini. Hereafter we use H and K, respectively, for the calibrated magnitudes in the Gemini photometry, $m_{\rm F205W}$ and $m_{\rm F160W}$. Fig. 2 shows the differences in magnitudes and colors between the *NICMOS* and the Gemini for the stars used for the transformation. Relatively large scatters seen in Fig. 2 appear to be due to the variation of the PSFs and the difference in the filters of the two systems.

Table A1 lists the photometry of the 327 measured bright stars ($K < 17$) of the Arches cluster. The X and Y coordinates listed in Table A1 are given in units of the pixel which corresponds to 0.02 arcsec. X increases to the west and Y increases to the north in Fig. 1(left). Some bright stars are labeled for identification in Fig. 1(left).

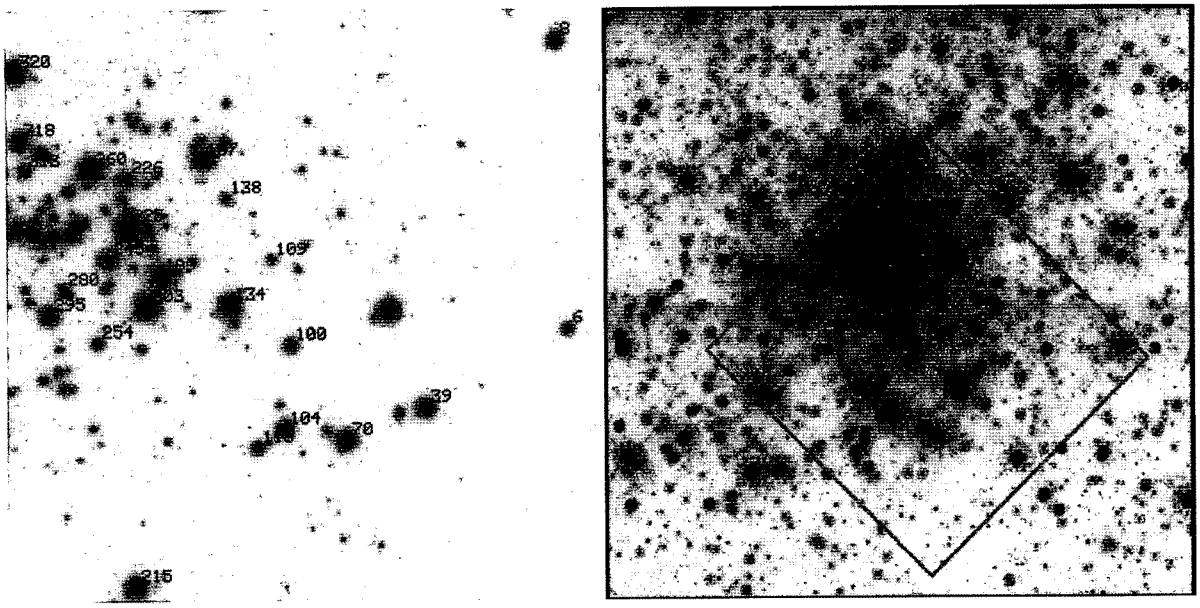

Fig. 1.— (Left) A gray scale map of the Gemini K' band image. The size of the field of view is $20''.5 \times 20''.5$. North is up and east is to the left. (Right) A gray scale map of the *HST/NICMOS* $K(F205W)$ band image. The solid line represents the Gemini field shown in the left.

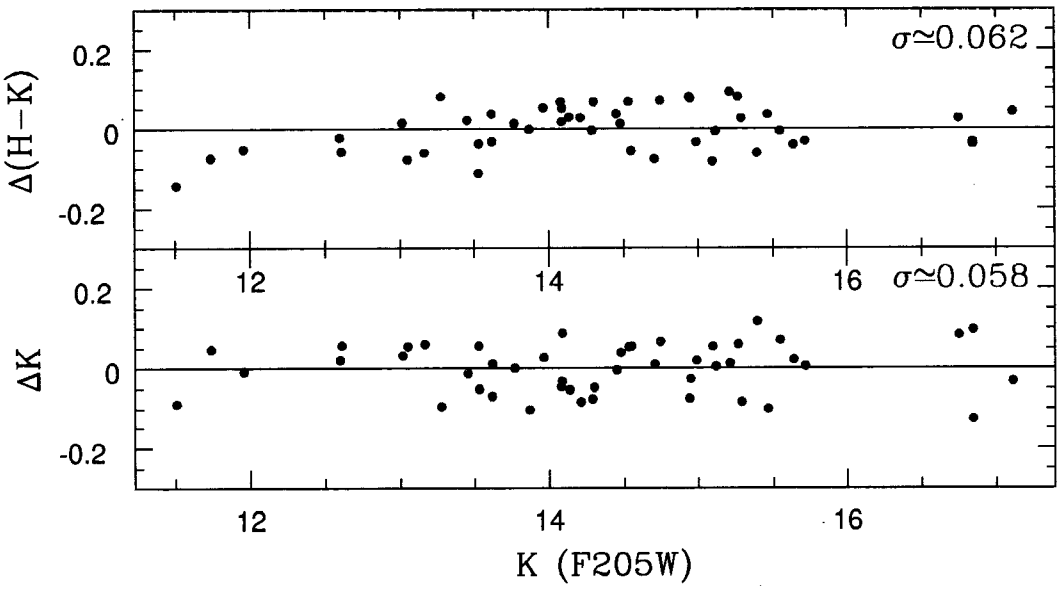

Fig. 2.— The differences in magnitudes and colors between the *NICMOS* photometry and the Gemini photometry for bright stars. The differences are given in terms of Δ = *NICMOS* photometry minus Gemini photometry.

III. Color-Magnitude Diagram

We display a color-magnitude diagram (CMD) of the measured stars in the Arches cluster in Fig. 3. Fig. 3 shows that most of the stars in the Arches cluster which corresponds to the upper main sequence of massive stars, indicating a very young age for the Arches cluster. The mean color of the main sequence is $(H-K) \approx 1.8$. Almost all the stars in the Gemini field are thought to be on the main sequence. The main sequence appears to be broadened due to a large amount of differential reddening that depends on the variable

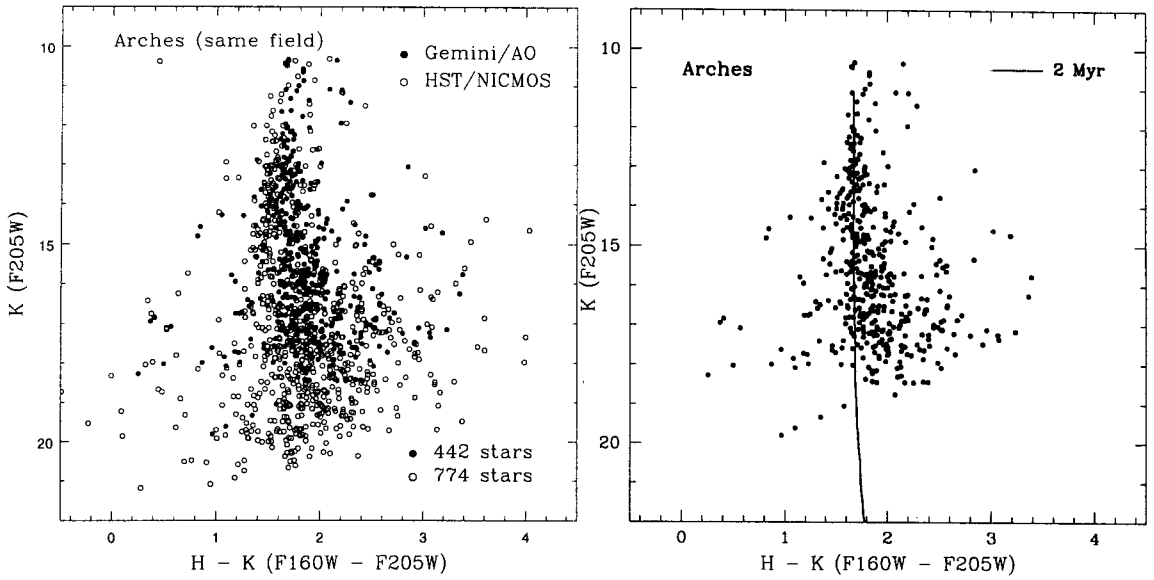

Fig. 3.—(Left) Color-magnitude diagram of the Arches cluster obtained from the Gemini data (filled circles) in comparison with *HST/NICMOS* results given by Figer et al. (1999) (open circles). (Right) Isochrone fits to the color-magnitude diagram of the Arches cluster. The solid line represents a 2 Myr isochrone from the Geneva models.

local extinction. For comparison, we have also plotted in Fig. 3 the *HST/NICMOS* photometry given by Figer et al. (1999) for the same field (marked by the square in Fig. 1.). Our CMD shows in general a good agreement with the *HST/NICMOS* results. However, the Gemini photometry is about 2 magnitude shallower than the HST photometry due to the shorter exposures of the Gemini H images.

In this study we adopt a distance modulus of $(m - M)_0 = -14.52$ (=8 kpc; Reid 1993) for the Arches cluster. For extinction correction, we use the mean color of the O-type stars in the cluster. We estimate the average color of the observed O-type star candidates with $12.0 < K < 15.0$ on the main sequence, obtaining a value of $(H - K) = 1.662$. Comparing this with the intrinsic color for O stars, $(H - K)_0 = -0.05$ (Panagia 1973), we derive an average color excess $E(H - K) = (H - K) - (H - K)_0 = 1.662 - (-0.05) = 1.712$. Using the extinction law of Rieke, Rieke, & Paul (1989), we derive an extinction value, $A_K = 1.95E(H-K) = 3.34$.

Then the age of the Arches cluster is estimated using the isochrones given by the Geneva group. Using the isochrones with $Z = 2Z_\odot$ and enhanced mass-loss rate (Meynet et al. 1994; Lejeune & Schaerer 2001), we derive approximately an age of $t_{age} \approx 2 \pm 1\ Myr$, as shown in the right panel of Fig. 3. This value is basically the same as the value given by Figer et al. (1999).

IV. LUMINOSITY FUNCTION

We have derived the luminosity function of the measured stars in the Arches cluster. To estimate incompleteness of our photometry, we have carried out the completeness test as follows. After adding artificial stars into the original frames, we have analyzed the resulting artificial frames in the same fashion as we applied to derive the photometry of the Arches cluster in the original images. We added only 50 stars to each image not to degrade the quality of the original images, and repeated the same process to create 400 artificial frames for each of H and K'. Our experiment was designed that the artificial stars follow random spatial distributions in each frame and that the LFs of the artificial stars follow the power law distributions. Table 2 lists the completeness of our photometry we derived thus. Table 2 shows that our photometry is more than 50% complete for $K < 18$ and $H < 19$.

Since K' images are much deeper than H images, we derive the luminosity functions of stars from each of K' and H photometry, rather than from the combination of both. We assume the mean color of the stars detected only in the K' images to be $(H - K) = 1.86$. Fig. 4 displays the K and H LFs derived from the Gemini images before incompleteness correction. The LFs derived from the *NICMOS* images for the same region as the Gemini field are also plotted for comparison. Fig. 4 shows that the LFs increase up to $K \approx 18$ and $H \approx 18$, and start decreasing thereafter. The turnover appears to be due to incompleteness of the Gemini photometry. It is found in Fig. 4 that the

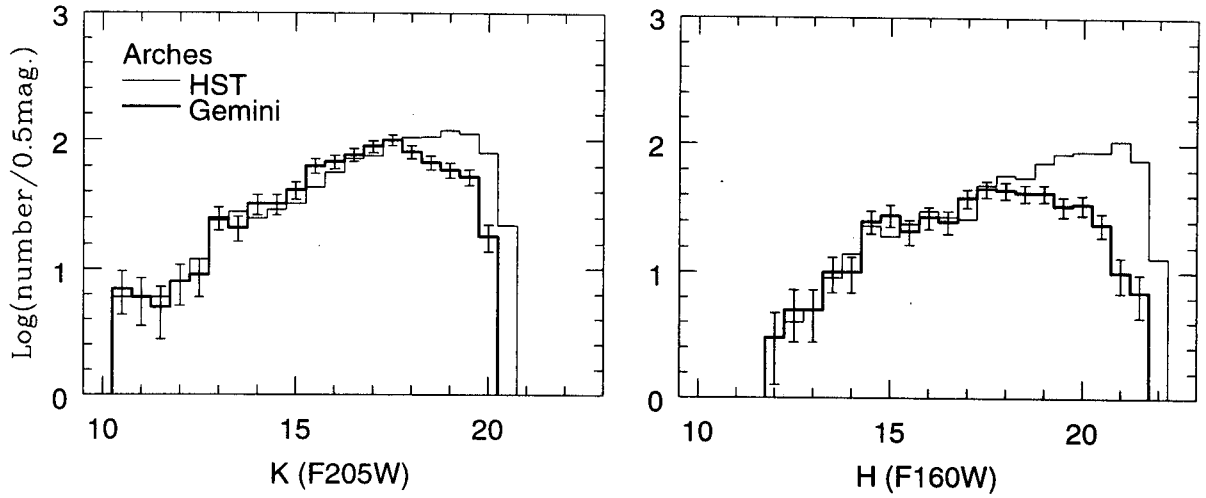

Fig. 4.— Luminosity functions of the Arches cluster derived from the Gemini H and K' images before incompleteness correction (thick lines with error bars). Light lines represent the LFs derived from the *NICMOS* data for the same area of the cluster.

Table 2. Completeness of our photometry

magnitude	F160W	F205W
12.5	1.00	1.00
13	1.00	0.99
13.5	1.00	0.99
14	0.98	0.94
14.5	0.94	0.93
15	0.97	0.92
15.5	0.92	0.88
16	0.89	0.82
16.5	0.86	0.75
17	0.86	0.71
17.5	0.77	0.60
18	0.74	0.51
18.5	0.65	0.41
19	0.53	0.29
19.5	0.39	0.18
20	0.27	0.13
20.5	0.16	0.05
21	0.09	0.01

Gemini LFs are very similar to the NICMOS LFs for $K < 18$ and $H < 18$.

Since the Gemini field is so small that there is little area which can be used as a control field for deriving the LFs of the cluster. Therefore we have used the *NICMOS* data for deriving the LFs of the control field which can be used for estimation of the field stars in the Gemini data. Although the characteristics of the Gemini data and the *NICMOS* data are different, the incompleteness-corrected LFs can be used approximately as a useful guide. We selected the outer regions at $r > 9''.5$ from the center of the cluster in the *NICMOS* images as a control field. The ratio of the area of the cluster field to that of the control field is 2.77, which is used for normalizing the LFs of the cluster region. The data for the incompleteness of the *NICMOS* photometry were provided by Figer et al. (1999). Fig. 5 (Upper panels) shows the incompleteness-corrected LFs of the control field thus derived and the LFs of the Arches cluster (thick lines with error bars). In the lower panels of Fig. 5 we display the LFs of the Arches cluster after incompleteness correction and field star subtraction. We plot the LFs for $K < 18$ and $H < 19$ for which the completeness in our photometry is higher than 50 % in Fig. 5.

V. INITIAL MASS FUNCTION

Luminosity functions of stars in clusters can be used to derive the initial mass functions with which stars in clusters form. For deriving the IMF we have followed the similar procedures to those used by Figer et al. (1999). We have converted the K-band LF derived in the previous section to the IMF, using the Geneva isochrone with an age of 2 Myrs as derived above. Fig. 6 shows the resulting IMF of the Arches cluster. Fitting a single power-law to the data, we derive a value for the slope of the IMF, $\Gamma = -0.79 \pm 0.16$ for the range of $1.0 < \log\ (M/M_{\odot}) < 2.1$. This value is in good agreement with the result based on the *HST/NICMOS* data, $\Gamma_{0.8-2.1} = -0.7 \pm 0.1$, derived by Figer et al. (1999). This result confirms that the IMF of the Arches cluster is indeed much flatter than that of the solar neighborhood which has an average value between $\Gamma = -1$ and $\Gamma = -2$ (Scalo 1998).

This result is also consistent with a recent finding based on the *HST/WFPC2* data that the IMFs of

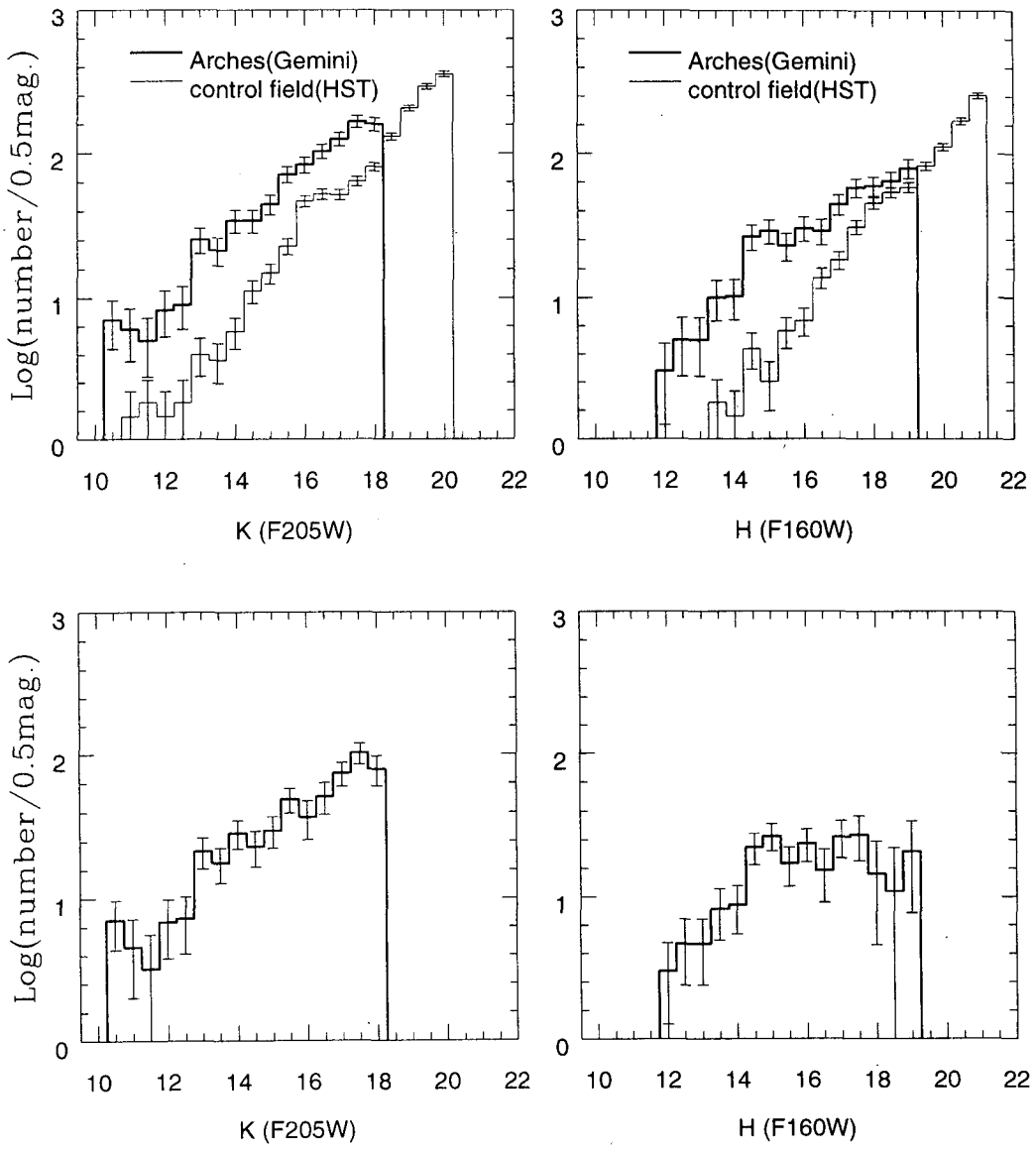

Fig. 5.— Luminosity functions of the Arches cluster after incompleteness correction. (Upper panels) The LFs of the Arches cluster derived from the Gemini H and K' images (thick lines with error bars). The LFs of the control field derived from the *NICMOS* data with the same area as the Gemini field are also plotted for comparison. (Lower panels) The LFs of the Arches cluster after subtraction of field contamination using the *NICMOS* data for the control field.

the bright stars in young clusters in M33 get flatter as the galactocentric distance decreases (Lee et al. 2001). This trend for the IMF depending on the galactocentric radius is not completely understood by any single theory until now, requiring detailed theoretical studies in the future. However, it may be explained by the photoevaporative process which provides a viable mechanism for ablating massive protostellar cores. In a dense environment where mass segregation occurs, massive stars in the more metal-rich center suffer less from ablation than low-mass stars. As a result, the IMFs get steeper, as the galactocentric radius increases and as the metallicity decreases (see Waller et al. 2002 for details). This result leads to a prediction that the

most top-heavy (the flattest) IMFs may occur near the metal-rich centers of star-forming galaxies (Lee et al. 2001).

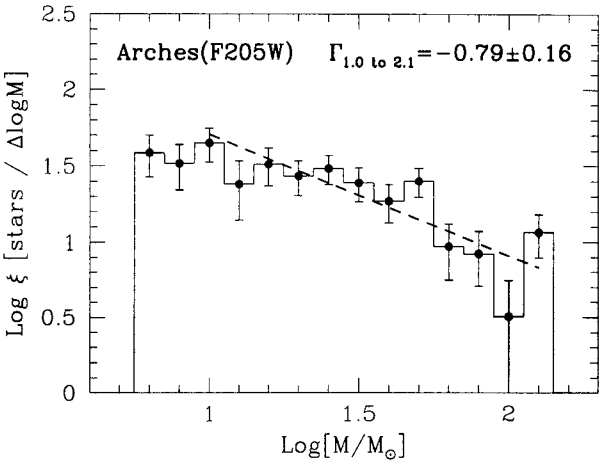

Fig. 6.— Initial mass function of the Arches cluster derived from the K images. The dashed line represents a fit to the data for the range of $1.0 < \log\ (M/M_\odot) < 2.1$.

VI. SUMMARY

We present Near-IR photometry of the Arches cluster near the Galactic center, using the data obtained for scientific demonstration with the Gemini/AO. Primary results are summarized as follows: First, the color-magnitude diagram of the Arches cluster shows a dominant blue main sequence consisting mainly of massive stars. Second, the age of the Arches cluster is estimated to be 2 ± 1 Myrs, using the Geneva isochrones. This value is consistent with that based on the *HST/NICMOS* data (Figer et al. 1999). Third, the K and H luminosity functions of the bright stars in the Arches clusters are derived, showing a slow increase toward the faint end. Fourth, the initial mass function of the massive stars with $1.0 < \log\ (M/M_\odot) < 2.1$ is derived. Fitting the power law to the data, we obtain a value for the IMF slope, $\Gamma = -0.79 \pm 0.16$. This confirms that Figer et al. (1999)'s result that the IMF of the Arches cluster is much flatter than that of the solar neighborhood. Although the *HST* provides unprecedented spatial resolution for the dense region, our results show that the ground-based AO systems in the Gemini telescope can yield comparable scientific results with some limits.

ACKNOWLEDGEMENTS

Based on observations obtained at the Gemini Observatory, which is operated by the Association of Universities for Research in Astronomy, Inc., under a cooperative agreement with the NSF on behalf of the Gemini partnership: the National Science Foundation (United States), the Particle Physics and Astronomy Research Council (United Kingdom), the National Research Council (Canada), CONICYT (Chile), the Australian Research Council (Australia), CNPq (Brazil) and CONICET (Argentina). We wish to thank Donald F. Figer for providing the *NICMOS* photometry data and helpful comments. The authors are grateful to the anonymous referee for useful suggestions. This work was supported in part by the Korea Research Foundation Grant (KRF-2000-DP0450) (to MGL).

REFERENCES

Blum, R. D., Schaerer, D., Pasquali, A., Heydari-Malayeri, M., Conti, P. S., & Schmutz, W. 2001, 2μm Narrow-band Adaptive Optics Imaging in the Arches Cluster, AJ, 122, 1875

Figer, D. F., Kim, S. S., Morris, M., Serabyn, E., Rich, R. M., & McLean, I. 1999, *HubbleSpaceTelescope/NICMOS* Observations of Massive Stellar Clusters near the Galactic Center, ApJ, 525, 750

Kim, S. S., Figer, D. F., Lee, H. M., & Morris, M. 2000, N-Body Simulations of Compact Young Clusters near the Galactic Center, ApJ, 545, 301

Lee, M. G., Park, H. S., Kim. S. C., Waller, W. H., Parker, J. W., Malumuth, E., & Hodge, P. 2001, *HST−WFPC2* Observations of the Star Clusters in the Giant HII Regions of M33, astro-ph 0109258

Lejeune, T., & Schaerer, D. 2001, Database of Geneva Stellar Evolution Tracks and Isochrones for UBVRI JHKLL'M, *HST − WFPC2*, Geneva, and Washington systems, A&A, 366, 538

Meynet, G., Maeder, A., Schaller, G.,Scahaerer, D., & Charbonnel, C. 1994, Grids of massive stars with high mass loss rates. V. From 12 to 120 $M_\odot$ at Z=0.001, 0.004, 0.008, 0.020 and 0.040, A&AS, 103, 97

Nagata, T., Woodward, C. E., Shure, M., & Kobayashi, N. 1995, Object 17: Another Cluster of Emission-Line Stars Near the Galactic Center, AJ, 109, 1676

Panagia, N. 1973, Some Physical parameters of early-type stars, AJ, 78, 929

Reid, M. J. 1993, The distance to the center of the Galaxy, ARA&A, 31, 345

Rieke, G. H.,Rieke, M. J., & Paul, A. E. 1989, Origin of the excitation of the galactic center, ApJ, 336, 752

Salpeter, E. E. 1955, The Luminosity Function and Stellar Evolution, ApJ, 121, 161

Scalo, J. 1998, The IMF Revisted: A Case for Variations, ASP Conf. Ser., 142, The Stellar Initial Mass Function, ed., G. Gilmore & D. Howell, 201

Stetson, P. 1987, DAOPHOT - A computer program for crowded-field stellar photometry, PASP, 99, 191

Stolte, A., Grebel, E. K., Brandner, W., & Figer, D. F. 2002, The Mass Function of the Arches Cluster from Gemini Adaptive Optics Data, astro-ph 0206360

Waller, W. H., Lee, M. G., Park, H. S., Kim, S. C. et al. 2002, Systematic IMF Variations in the Giant HII Regions of M33, in preparation

Yang, Y., Park, H. S., Lee, M. G., & Lee, S.-G. 2002, Near-IR Photometry of the Arches Cluster close to the Galactic Center, Bull. of Korean Astro. Soc., 27, 50

Yuzef-Zadeh, F., Law, C., Wardle, M., Wang, Q. D., Fruscione, A., Lang, C. C., & Cotera, A. 2002, Detection of X-ray Emissioin from the Arches Cluster Near the Galactic Center, ApJ, 570, 665

Tablel A1. *HK* Photometry of the Arches cluster

ID	X	Y	$m_{\rm F160W}$	$\sigma_{\rm F160W}$	$m_{\rm F205W}$	$\sigma_{\rm F205W}$
1	13.31	798.29	18.458	0.018	16.549	0.007
2	13.48	877.90	18.203	0.015	16.239	0.007
3	24.36	299.74	19.408	0.032	16.868	0.016
4	25.32	106.45	19.422	0.030	16.906	0.010
5	29.01	550.91	19.154	0.019	15.768	0.004
6	65.87	466.82	14.142	0.001	11.948	0.001
7	66.83	186.00	19.449	0.026	16.734	0.007
8	85.05	964.18	13.705	0.005	11.420	0.001
9	85.82	613.33	17.312	0.009	16.941	0.006
10	90.75	915.24	18.510	0.020	16.689	0.010
11	113.81	878.84	18.015	0.009	16.128	0.004
12	116.73	604.14	18.966	0.018	16.601	0.005
13	135.46	900.71	18.685	0.019	16.642	0.009
14	137.13	159.57	18.959	0.019	16.778	0.006
15	141.28	628.29	18.011	0.008	15.967	0.003
16	155.80	884.66	18.416	0.012	16.577	0.006
17	160.11	577.34	18.063	0.008	15.529	0.003
18	167.72	667.00	18.362	0.011	16.502	0.004
19	172.04	867.77	19.025	0.019	16.890	0.006
20	174.60	85.83	18.894	0.017	16.678	0.005
21	180.03	745.25	17.703	0.007	16.021	0.004
22	195.30	495.61	18.630	0.011	16.125	0.003
23	215.71	370.56	17.908	0.006	14.721	0.002
24	217.64	141.69	19.063	0.021	16.864	0.006
25	227.92	639.15	18.432	0.010	16.258	0.004
26	241.55	677.38	18.646	0.015	16.318	0.005
27	246.42	388.05	18.769	0.020	16.894	0.011
28	248.56	784.94	15.531	0.001	13.633	0.001
29	248.79	662.92	17.004	0.005	15.152	0.003
30	251.56	211.32	17.739	0.006	15.725	0.003
31	263.63	365.80	18.269	0.014	16.244	0.005
32	266.06	517.45	16.571	0.003	14.585	0.002
33	282.63	997.29	17.880	0.009	15.864	0.004
34	282.96	685.03	18.462	0.012	16.794	0.006
35	285.46	246.33	18.416	0.011	16.247	0.004
36	285.47	177.83	17.833	0.008	15.770	0.003
37	297.76	404.94	18.282	0.013	16.211	0.007
38	304.65	964.61	18.300	0.012	16.613	0.006
39	310.57	333.01	13.173	0.003	11.091	0.002
40	313.51	818.23	17.643	0.006	15.827	0.003
41	318.94	658.65	16.705	0.005	15.009	0.003
42	325.35	678.74	17.557	0.008	15.826	0.005
43	346.69	639.08	16.350	0.003	14.685	0.002
44	351.02	410.35	18.756	0.018	16.877	0.008
45	356.20	985.03	17.220	0.006	15.265	0.003
46	357.48	323.85	14.579	0.003	12.618	0.002
47	359.89	313.05	17.509	0.016	15.545	0.008
48	363.00	592.65	16.355	0.004	14.683	0.002
49	363.23	583.24	17.094	0.008	15.411	0.003
50	364.02	77.42	18.556	0.025	16.962	0.018
51	365.38	938.78	17.944	0.008	16.270	0.004
52	373.63	895.37	17.725	0.008	16.072	0.004
53	385.82	902.26	16.100	0.004	14.446	0.003
54	388.88	750.41	17.500	0.005	15.661	0.002
55	390.60	97.36	15.281	0.002	13.768	0.001
56	393.77	567.25	17.133	0.018	15.728	0.008
57	397.01	347.02	18.576	0.026	16.667	0.016
58	400.25	66.41	18.856	0.144	16.562	0.106
59	401.67	485.62	15.066	0.128	13.640	0.094
60	402.46	690.07	17.498	0.006	15.722	0.003

Tablel A1. continued.

ID	X	Y	m_{F160W}	σ_{F160W}	m_{F205W}	σ_{F205W}
61	410.87	992.19	17.896	0.010	15.882	0.005
62	422.47	940.35	19.051	0.022	16.884	0.007
63	423.33	871.85	18.112	0.012	16.500	0.005
64	428.48	865.46	18.795	0.022	16.944	0.008
65	429.51	233.92	17.552	0.022	15.743	0.012
66	431.58	128.76	18.436	0.015	16.385	0.006
67	436.16	678.00	18.490	0.019	16.523	0.010
68	439.35	862.51	18.422	0.015	16.503	0.008
69	442.54	615.97	17.357	0.006	15.511	0.003
70	446.08	278.43	13.310	0.003	11.108	0.002
71	447.95	766.26	18.507	0.019	16.729	0.011
72	449.92	990.33	17.442	0.006	15.013	0.003
73	455.22	107.64	16.278	0.003	13.771	0.001
74	455.44	667.17	14.880	0.003	13.104	0.002
75	459.78	256.61	16.637	0.049	14.818	0.035
76	461.76	770.70	15.517	0.004	13.794	0.003
77	462.74	281.99	16.341	0.018	14.128	0.012
78	462.89	703.99	18.661	0.020	16.932	0.012
79	463.34	153.75	17.249	0.006	14.810	0.003
80	475.28	754.90	18.405	0.027	16.809	0.016
81	475.72	235.36	16.899	0.020	14.947	0.014
82	479.80	657.60	16.931	0.006	15.122	0.004
83	480.31	175.97	16.900	0.005	14.866	0.003
84	482.30	294.59	14.978	0.003	12.971	0.002
85	484.29	773.87	15.774	0.003	13.992	0.002
86	492.61	333.23	17.854	0.009	15.347	0.005
87	493.89	989.12	18.565	0.015	16.769	0.007
88	495.94	677.95	17.807	0.009	16.031	0.005
89	504.33	939.50	19.034	0.020	16.876	0.007
90	508.58	126.87	17.626	0.005	14.606	0.002
91	511.99	825.72	15.284	0.001	13.550	0.001
92	514.87	151.05	18.162	0.009	15.327	0.003
93	516.07	613.71	15.279	0.003	13.585	0.002
94	521.21	741.74	15.416	0.003	13.443	0.002
95	524.83	255.82	16.234	0.004	14.253	0.003
96	530.13	570.78	14.903	0.003	13.223	0.002
97	533.13	465.32	17.722	0.018	15.693	0.012
98	533.49	738.87	18.047	0.009	15.478	0.003
99	536.74	488.22	17.266	0.006	15.562	0.003
100	543.28	440.70	13.604	0.001	11.783	0.001
101	544.92	209.91	17.922	0.008	16.002	0.004
102	551.63	764.89	18.464	0.014	16.718	0.006
103	553.40	26.72	16.851	0.006	14.517	0.003
104	553.84	297.10	13.250	0.003	11.366	0.002
105	555.33	677.58	17.743	0.007	15.943	0.003
106	558.03	248.77	18.130	0.035	16.367	0.015
107	562.75	339.36	15.237	0.007	13.412	0.005
108	569.55	979.09	17.198	0.006	15.542	0.003
109	575.94	586.78	14.399	0.003	12.666	0.002
110	580.95	275.17	15.934	0.021	14.056	0.015
111	581.11	484.14	18.286	0.016	16.561	0.009
112	584.44	500.77	18.471	0.018	16.698	0.010
113	593.32	347.65	18.050	0.017	16.051	0.009
114	594.23	780.81	18.438	0.013	16.697	0.006
115	601.06	265.02	13.955	0.003	12.067	0.002
116	601.92	183.67	17.617	0.006	15.731	0.003
117	605.02	351.85	17.239	0.019	16.833	0.013
118	606.15	635.89	16.468	0.004	14.767	0.002
119	606.85	666.02	15.802	0.007	14.177	0.004
120	616.94	217.67	17.823	0.011	15.967	0.005

Tablel A1. continued.

ID	X	Y	m_{F160W}	σ_{F160W}	m_{F205W}	σ_{F205W}
121	618.52	438.86	16.282	0.003	14.538	0.002
122	624.19	196.86	19.538	0.027	16.866	0.007
123	624.90	771.86	16.392	0.016	14.684	0.009
124	626.30	536.89	16.543	0.081	14.488	0.058
125	629.25	390.83	18.839	0.027	16.704	0.016
126	631.96	903.09	17.915	0.008	15.444	0.004
127	633.77	462.13	17.800	0.028	16.375	0.015
128	637.38	747.37	18.173	0.027	16.556	0.013
129	637.52	408.21	18.502	0.016	16.770	0.009
130	638.40	447.58	17.514	0.010	15.629	0.006
131	639.51	478.27	14.976	0.013	13.188	0.008
132	640.88	684.52	17.401	0.019	15.431	0.007
133	644.45	99.42	18.188	0.009	15.715	0.003
134	646.61	510.09	12.402	0.016	10.576	0.012
135	646.89	588.43	17.991	0.014	16.196	0.008
136	648.01	569.27	17.377	0.008	15.663	0.005
137	650.17	857.43	14.825	0.004	13.048	0.003
138	653.28	693.10	14.166	0.003	12.522	0.002
139	653.55	742.92	17.947	0.031	16.408	0.013
140	654.98	787.46	13.729	0.004	12.051	0.003
141	655.00	469.41	17.175	0.036	15.621	0.023
142	656.24	29.89	18.720	0.017	16.340	0.006
143	657.38	647.81	18.857	0.025	16.263	0.010
144	659.93	454.88	16.529	0.012	14.722	0.008
145	660.06	270.11	16.702	0.006	14.923	0.003
146	661.27	614.38	19.432	0.060	16.988	0.021
147	667.98	814.95	16.891	0.029	15.450	0.014
148	668.30	943.29	17.514	0.032	15.713	0.022
149	668.86	447.54	18.108	0.020	16.243	0.013
150	671.97	768.86	15.934	0.031	14.431	0.016
151	672.06	526.71	17.283	0.156	15.640	0.111
152	672.31	752.37	16.176	0.041	14.605	0.021
153	676.64	495.21	16.790	0.085	14.682	0.059
154	681.79	80.01	19.105	0.021	16.532	0.006
155	688.05	794.04	15.687	0.021	14.196	0.012
156	692.85	502.65	17.815	0.024	16.212	0.012
157	693.27	759.10	12.784	0.009	10.999	0.006
158	696.37	282.54	18.161	0.009	16.219	0.004
159	697.19	795.21	15.200	0.013	13.523	0.008
160	703.22	722.71	16.976	0.041	15.061	0.013
161	704.72	829.84	15.325	0.005	14.274	0.003
162	707.79	783.73	15.393	0.081	13.781	0.058
163	708.27	648.67	16.487	0.007	14.777	0.003
164	710.86	629.52	18.164	0.021	16.218	0.009
165	711.18	586.78	14.465	0.004	12.820	0.003
166	712.26	361.57	15.976	0.003	14.213	0.002
167	713.32	288.74	19.047	0.022	16.691	0.006
168	715.42	966.03	17.313	0.010	15.708	0.006
169	718.15	616.15	17.764	0.025	15.764	0.010
170	719.81	634.91	16.576	0.009	14.871	0.005
171	720.45	508.98	15.587	0.004	13.955	0.003
172	720.98	413.27	17.711	0.008	15.899	0.004
173	728.83	309.28	17.563	0.009	15.618	0.005
174	729.75	910.69	17.451	0.008	15.508	0.004
175	737.36	964.41	17.739	0.012	15.954	0.007
176	737.48	841.70	17.830	0.033	16.487	0.017
177	738.99	643.67	18.424	0.038	16.230	0.015
178	740.72	534.85	17.129	0.058	15.947	0.024
179	740.83	567.82	15.904	0.021	13.059	0.006
180	748.48	650.27	17.649	0.024	15.773	0.010

Tablel A1. continued.

ID	X	Y	$m_{\rm F160W}$	$\sigma_{\rm F160W}$	$m_{\rm F205W}$	$\sigma_{\rm F205W}$
181	749.07	692.04	16.228	0.005	14.571	0.003
182	749.17	958.63	18.973	0.024	16.597	0.007
183	753.10	817.83	14.627	0.006	13.037	0.004
184	756.08	277.13	15.385	0.002	13.481	0.001
185	757.43	663.90	16.444	0.013	14.779	0.008
186	758.81	646.54	15.543	0.007	13.871	0.004
187	760.51	230.36	18.510	0.017	16.600	0.006
188	763.07	475.47	16.521	0.041	15.060	0.023
189	766.93	560.10	12.478	0.012	10.653	0.009
190	767.16	43.01	17.064	0.008	14.889	0.004
191	767.94	77.74	17.605	0.009	15.751	0.005
192	768.08	738.11	15.635	0.009	14.069	0.004
193	771.23	666.77	15.835	0.014	14.288	0.008
194	771.84	732.37	15.565	0.011	13.994	0.004
195	772.12	349.48	15.840	0.003	14.035	0.002
196	775.10	604.65	15.727	0.013	13.945	0.005
197	777.59	28.75	16.441	0.084	14.376	0.058
198	778.33	252.17	17.129	0.007	15.207	0.004
199	781.91	608.80	15.007	0.007	13.254	0.004
200	783.68	365.22	19.072	0.021	16.496	0.005
201	784.09	893.65	15.034	0.007	13.374	0.004
202	787.71	639.47	13.973	0.011	12.362	0.004
203	787.97	508.09	12.014	0.024	10.330	0.017
204	788.50	813.02	14.778	0.007	13.131	0.004
205	788.52	916.38	17.560	0.023	15.738	0.012
206	790.63	717.61	15.187	0.013	13.826	0.005
207	792.42	309.39	17.937	0.016	16.097	0.010
208	793.41	650.32	15.549	0.041	14.291	0.021
209	800.05	435.34	14.600	0.004	12.908	0.003
210	800.19	137.19	16.486	0.003	14.714	0.002
211	801.25	905.26	17.888	0.045	16.571	0.025
212	801.34	858.01	16.244	0.009	14.595	0.005
213	805.14	649.16	14.270	0.031	12.886	0.021
214	805.31	830.31	15.429	0.009	13.920	0.005
215	810.92	27.20	12.701	0.007	10.871	0.004
216	812.34	819.37	15.206	0.007	13.666	0.004
217	812.64	760.87	16.932	0.042	15.786	0.014
218	812.81	950.65	18.041	0.016	16.350	0.008
219	813.73	574.82	15.322	0.023	13.597	0.010
220	815.14	613.09	16.189	0.040	13.932	0.009
221	817.73	489.09	17.091	0.056	15.227	0.027
222	817.82	834.25	15.144	0.008	13.583	0.005
223	818.71	981.20	16.936	0.009	15.223	0.005
224	820.13	883.59	16.606	0.011	15.162	0.006
225	820.78	645.88	12.110	0.021	10.450	0.015
226	821.65	727.77	13.281	0.005	11.660	0.003
227	822.74	626.38	14.682	0.017	13.060	0.008
228	827.86	500.51	18.111	0.163	16.353	0.107
229	830.03	482.47	17.063	0.017	15.093	0.007
230	830.43	690.31	14.905	0.008	13.277	0.003
231	832.54	428.57	17.966	0.032	16.719	0.012
232	833.20	925.02	18.052	0.016	16.557	0.009
233	839.20	695.70	16.137	0.021	14.525	0.008
234	842.80	794.44	15.882	0.010	14.104	0.005
235	843.15	724.21	15.934	0.033	14.325	0.018
236	843.73	85.36	18.965	0.024	16.949	0.009
237	846.15	499.58	17.972	0.063	16.746	0.044
238	847.47	874.16	17.989	0.029	16.347	0.017
239	849.41	931.26	17.106	0.010	15.466	0.006
240	849.42	831.54	15.487	0.014	13.913	0.009

Tablel A1. continued.

ID	X	Y	$m_{\rm F160W}$	$\sigma_{\rm F160W}$	$m_{\rm F205W}$	$\sigma_{\rm F205W}$
241	849.50	261.85	18.114	0.013	16.266	0.007
242	849.58	791.78	16.993	0.022	15.387	0.010
243	851.58	513.50	16.615	0.010	14.882	0.005
244	853.22	547.72	15.350	0.007	13.722	0.004
245	854.93	589.08	13.030	0.006	11.325	0.004
246	856.95	97.14	17.736	0.009	15.890	0.005
247	858.18	748.40	15.623	0.116	14.805	0.081
248	858.70	502.00	16.622	0.012	14.922	0.007
249	860.44	674.43	15.209	0.006	13.444	0.003
250	861.72	538.09	14.633	0.004	12.966	0.003
251	864.41	471.32	16.409	0.014	14.836	0.005
252	868.72	805.45	16.829	0.022	15.166	0.014
253	871.63	273.18	15.915	0.004	14.129	0.002
254	874.66	446.09	13.998	0.004	12.253	0.003
255	878.82	564.91	17.562	0.114	15.948	0.079
256	880.10	323.68	17.429	0.012	15.684	0.006
257	881.72	368.54	17.907	0.012	16.058	0.004
258	883.71	108.47	18.676	0.019	16.501	0.007
259	883.74	300.12	14.986	0.003	13.182	0.002
260	884.08	743.84	12.083	0.019	10.433	0.014
261	893.80	504.37	18.420	0.074	16.788	0.051
262	896.40	652.41	14.751	0.009	13.240	0.005
263	896.96	180.75	18.019	0.012	16.214	0.007
264	906.31	550.05	17.708	0.051	16.407	0.019
265	906.42	246.61	15.883	0.003	14.084	0.002
266	906.71	486.06	18.086	0.038	15.758	0.010
267	908.12	891.75	17.991	0.014	16.446	0.008
268	910.00	646.73	13.628	0.008	11.969	0.005
269	910.60	60.84	17.819	0.009	16.020	0.005
270	917.22	669.23	16.380	0.031	14.516	0.012
271	919.78	368.80	15.019	0.008	13.288	0.005
272	921.10	629.91	14.064	0.009	12.418	0.005
273	921.43	302.65	17.091	0.007	15.366	0.004
274	923.20	529.83	15.801	0.015	14.221	0.007
275	923.99	706.39	14.258	0.008	12.584	0.005
276	925.19	861.50	16.949	0.010	15.264	0.006
277	926.63	401.45	16.060	0.010	14.347	0.005
278	929.85	149.43	15.845	0.004	14.053	0.003
279	931.02	930.44	18.062	0.015	16.340	0.009
280	932.75	537.29	13.753	0.005	12.081	0.003
281	934.90	368.20	14.514	0.005	12.800	0.003
282	935.24	437.87	17.103	0.022	15.317	0.009
283	936.27	599.77	16.664	0.034	14.633	0.010
284	937.49	453.60	17.037	0.015	15.380	0.009
285	940.69	231.90	18.014	0.012	16.052	0.005
286	942.63	435.84	15.262	0.006	13.581	0.003
287	942.76	397.20	14.546	0.005	12.862	0.003
288	943.69	786.33	15.918	0.018	14.250	0.008
289	944.01	905.80	17.933	0.024	16.745	0.011
290	948.37	627.94	14.066	0.008	12.387	0.005
291	949.03	226.44	16.985	0.007	15.157	0.004
292	949.47	661.04	15.120	0.099	13.551	0.072
293	950.85	566.41	17.719	0.042	15.781	0.016
294	955.49	761.76	15.918	0.026	14.542	0.015
295	956.86	493.98	12.897	0.006	11.132	0.004
296	957.71	691.24	15.138	0.009	13.434	0.005
297	964.21	237.82	16.577	0.005	14.809	0.003
298	969.32	383.76	14.501	0.005	12.788	0.003
299	969.91	773.09	13.857	0.010	12.226	0.006
300	970.23	623.74	14.104	0.008	12.367	0.005

Tablel A1. continued.

ID	X	Y	$m_{\rm F160W}$	$\sigma_{\rm F160W}$	$m_{\rm F205W}$	$\sigma_{\rm F205W}$
301	970.40	675.82	15.957	0.013	14.118	0.006
302	970.58	588.81	15.561	0.014	14.053	0.006
303	978.28	632.56	14.704	0.012	13.085	0.006
304	980.00	656.26	15.025	0.013	13.302	0.007
305	980.40	901.56	15.487	0.037	14.059	0.020
306	982.36	573.15	17.849	0.046	15.690	0.017
307	987.45	132.59	19.609	0.031	16.251	0.009
308	988.40	634.39	14.855	0.013	13.144	0.007
309	989.04	806.84	15.414	0.108	14.571	0.075
310	989.66	12.73	18.499	0.023	16.634	0.013
311	991.39	517.55	14.650	0.007	13.011	0.004
312	998.25	862.62	16.698	0.016	15.322	0.007
313	998.83	741.32	13.886	0.010	12.178	0.006
314	998.86	538.89	14.766	0.007	12.981	0.005
315	999.75	122.03	18.580	0.019	16.616	0.011
316	1002.16	694.80	15.729	0.098	13.966	0.072
317	1006.10	311.77	17.149	0.028	15.651	0.016
318	1006.72	793.98	12.763	0.012	11.104	0.008
319	1012.71	642.70	13.342	0.009	11.632	0.006
320	1013.21	912.36	12.507	0.022	10.354	0.015
321	1013.92	370.78	16.861	0.013	14.881	0.005
322	1019.91	266.30	16.104	0.008	14.372	0.004
323	1021.98	167.92	17.561	0.010	15.726	0.006
324	1025.87	364.09	14.810	0.006	13.173	0.004
325	1027.45	510.86	16.142	0.012	14.163	0.005
326	1028.92	427.06	17.048	0.009	15.267	0.005
327	1033.92	158.94	18.613	0.032	16.846	0.015